The American Journal of Pathology, Vol. 174, No. 3, March 2009

DOI: 10.2353/ajpath.2009.080625

Vascular Biology, Atherosclerosis and Endothelium Biology

Chloride Intracellular Channel Protein-4 Functions in Angiogenesis by Supporting Acidification of Vacuoles Along the Intracellular Tubulogenic Pathway

Barbara Ulmasov,* Jonathan Bruno,[†‡] Nicarter Gordon,[†‡] M. Elizabeth Hartnett,[§] and John C. Edwards[†]

From the Department of Medicine, St. Louis University, St. Louis, Missouri; and the University of North Carolina Kidney Center,[†] and the Departments of Medicine,[‡] and Ophthalmology,[§] University of North Carolina, Chapel Hill, North Carolina*

Endothelial cells form capillary tubes through the process of intracellular tubulogenesis. Chloride intracellular channel (CLIC) family proteins have been previously implicated in intracellular tubulogenesis, but their specific role has not been defined. In this study, we show that disruption of the *Clic4* gene in mice results in defective angiogenesis *in vivo* as reflected in a Matrigel plug angiogenesis assay. An angiogenesis defect is also apparent in the retina, both in the decreased spontaneous development of retinal vasculature of unstressed mice and in the dramatically decreased angiogenic response of retinal vessels to an oxygen toxicity challenge. We found that endothelial cells derived from *Clic4*$^{-/-}$ mice demonstrated impaired tubulogenesis in three-dimensional fibrin gels compared with cells derived from wild-type mice. Furthermore, we found that tubulogenesis of wild-type cells in culture was inhibited by both an inhibitor of CLICs and an inhibitor of the vacuolar proton ATPase. Finally, we showed that vacuoles along the endothelial tubulogenesis pathway are acidic in wild-type cells, and that vacuolar acidification is impaired in *Clic4*$^{-/-}$ cells while lysosomal acidification is intact. We conclude that CLIC4 plays a critical role in angiogenesis by supporting acidification of vacuoles along the cell-hollowing tubulogenic pathway. ***(Am J Pathol 2009, 174:1084–1096; DOI: 10.2353/ajpath.2009.080625)***

The ability of endothelial cells to organize into multicellular capillary tubes is essential to normal development and is important in disease states such as cancer and diabetes mellitus. Endothelial cells can form capillary tubes through the process of cell-hollowing tubulogenesis that involves the coordinated formation and fusion of specialized intracellular vacuoles.[1,2] During cell-hollowing tubulogenesis, cells form a large intracellular lumen through the fusion of multiple intracellular vesicles.[1] This lumen then fuses with those of neighboring cells and what was the lumen of the intracellular compartment becomes the extracellular lumen of the multicellular tube. Thus tubulogenesis of capillaries requires organized traffic of intracellular membranes. In addition to numerous other proteins,[3] ion transporters have been implicated in intracellular membrane traffic. In particular, acidification by the electrogenic vacuolar proton ATPase (vH-ATPase) coupled with a short-circuiting chloride conductance is important in trafficking of several intracellular compartments.[4]

CLICs are a family of proteins that have been implicated as intracellular chloride channels, but whose physiological roles remain uncertain.[5] A CLIC family member has been shown to be essential for the cell-hollowing tubulogenesis of the excretory cell of *Caenorhabditis elegans*[6] in which it is necessary for intracellular vesicles to fuse into an intact intracellular tube although its specific role in this process is unknown. Furthermore, CLIC4 (one of six mammalian CLICs) has been implicated in endothelial cell tubulogenesis in a proteomics study.[7]

To explore the physiological roles of CLIC4 more directly, we generated mice in which the *Clic4* gene has been disrupted. In this study, we report that *Clic4*$^{-/-}$ mice demonstrate decreased angiogenesis activity in

Supported by the Department of Veterans Affairs (merit award to J.C.E.), the National Institutes of Health (grants RO1 DK060551 to J.C.E. and R01 EY015130 to M.E.H.), and the Research to Prevent Blindness (to M.E.H.).

Accepted for publication November 24, 2008.

Address reprint requests to John C. Edwards, M.D., Ph.D., Associate Professor of Medicine and of Cell and Molecular Physiology, Campus Box 7155, University of North Carolina, Chapel Hill, NC 27514-7155. E-mail: jedwards@med.unc.edu.

two independent *in vivo* assays. Endothelial cells derived from these mice show decreased ability to proceed through the cell-hollowing tubulogenesis pathway, and cell-hollowing tubulogenesis of wild-type endothelial cells is inhibited both by IAA-94, a CLIC inhibitor,[8] and by bafilomycin A1, an inhibitor of the vacuolar proton ATPase.[9] We directly measured the pH of intracellular vacuoles along the cell-hollowing tubulogenesis pathway, showing that they acidify and that acidification is impaired in *Clic4*$^{-/-}$ cells. We conclude CLIC4 plays a critical role in angiogenesis by supporting acidification of vacuoles along the cell-hollowing tubulogenic pathway, perhaps by providing a short-circuiting ion conductance to permit transport by the electrogenic vacuolar proton pump. These data firmly identify CLIC4 as a key player in angiogenesis, identify vacuolar acidification as a necessary process in cell-hollowing tubulogenesis, and establish a novel specific physiological function for a member of a protein family whose cellular roles have been uncertain.

Materials and Methods

Animal studies were performed in accordance with the regulations of the institutional animal care and use committees. Matrigel plug experiments,[10,11] preparation of retinal flat mounts,[12] induction of retinal angiogenesis after hyperoxygen exposure,[13,14] isolation of heart endothelial cells,[15] and vacuolization assay in fibrin gels[16,17] were performed using published methods with slight modifications as described below.

Generation of New Antisera

The peptide CMALSMPLNGLKEED, which represents the N-terminal sequence of mouse CLIC4 with an N-terminal cysteine added, was covalently linked to keyhole limpet hemocyanin and the conjugate used to immunize a rabbit using the services of Cocalico Biologicals, Reamstown, PA. A high-titer antiserum was obtained and was affinity-purified over a column of recombinant CLIC4 immobilized on an AminoLink matrix (Pierce Biochemicals, Rockford, IL). The resulting affinity-purified antibody is named AP255. Western blot of glutathione *S*-transferase fusion proteins with CLIC1, CLIC4, and CLIC5 were performed as previously described.[18]

Generation of *Clic4*$^{-/-}$ Mice

Nucleotide coordinates are numbered from NCBI mouse genome sequences NT_039267. Fragments of CLIC4 gene were amplified from mouse genomic DNA using polymerase chain reaction (PCR). An upstream fragment (position 31,018 to 33,277) from intron 1 and downstream fragment (33,924 to 37,925) from intron 2 were inserted into the *Kpn*I-*Xba*I and *Xho*I-*Not*I sites of pNT-Cass-loxA (gift of Drs. Shunji Tomatsu and William Sly, St. Louis University, St. Louis, MO).[19]

The targeting vector was linearized at the *Not*I site and introduced into embryonic stem cells (line W9.5 derived from 129/Sv mice; Gene Targeting Services, Yale University, New Haven, CT) by electroporation using standard methods (Siteman Cancer Center Murine Embryonic Stem Cell Core, St. Louis, MO). Cells were selected for growth in G418 (400 μg/ml) and ganciclovir (2 μmol/L). Individual colonies were selected after 1 week, DNA isolated, and screened for homologous recombination by PCR. Positive colonies were confirmed by Southern blotting of *Nhe*I-digested genomic DNA. The Southern blot probe consisted of fragments 30,021 to 30,840 from the CLIC4 gene. Blastocyst injection and generation of chimeric offspring were performed by the Transgenic Core Facility at Washington University, St. Louis, MO. Animals were genotyped by PCR amplification of tail DNA. Primers for genotyping the CLIC4 lineage were 5′-TGACCACGGCAACTCCTAGAAGGACCGG-3′ and 5′-AGGAC TCGGGGTGACACTGTAAATCGAC-3′.

Histology and Immunostaining of Matrigel Plugs

Two weeks after injection, mice were sacrificed and Matrigel plugs were removed. Plugs for trichrome staining were fixed in 10% buffered formalin for 24 hours before embedding, sectioning, and staining. Plugs for lectin stain were fixed overnight in zinc fixative, embedded in paraffin, and sectioned. After deparaffinization through xylene and graded alcohols, sections were blocked for 1 hour in L-PBS (135 mmol/L NaCl, 10 mmol/L sodium phosphate, pH 7.4, 0.1 mmol/L $CaCl_2$, 0.1 mmol/L $MgCl_2$, 0.1 mmol/L $MnCl_2$) with 1% bovine serum albumin and 0.2% Triton X-100. Sections were incubated with Alexa Fluor 565-isolectin B4 (ILB4) from *Griffonia simplicifolia* (Invitrogen, Carlsbad, CA) at 10 μg/ml in L-PBS with 0.05% fish gelatin for 1 hour. The samples were washed four times for 5 minutes in L-PBS. The first wash contained 1 nmol/L Sytox Green (Invitrogen) to stain nuclei.

Assay of Hemoglobin Content of Matrigel Plugs

Plugs were homogenized in 100 mmol/L NaCl, 10 mmol/L Tris-HCl, pH 7.0, 1 mmol/L ethylenediaminetetraacetic acid, and 0.1 mmol/L phenylmethyl sulfonyl fluoride. Insoluble material was removed by centrifugation, re-extracted with water, and the supernatants pooled. Five μg of protein (determined by BCA assay) were separated by sodium dodecyl sulfate-polyacrylamide gel electrophoresis (SDS-PAGE), blotted, and probed with antibody to mouse hemoglobin (MP Biomedicals, Solon, OH) using the SuperSignal chemiluminescent detection system (Pierce Biochemicals) and detected with X-ray film. Intensity of signal was determined by densitometry using the GelDoc2000 instrument (Bio-Rad, Hercules, CA) with multianalyst software. *P* values were determined using Student's two-tailed *t*-test.[20]

Staining Retina Flat Mounts

Mice were sacrificed by CO_2 inhalation and eyes removed. For lectin stain, the whole eyes were fixed in 2%

paraformaldehyde in saline for 2 hours. Retinal whole mounts were incubated in ice-cold 70% methanol for 10 minutes, rinsed with phosphate-buffered saline (PBS), incubated in PBS with 1% Triton X-100 for 30 minutes, rinsed with PBS, incubated in Alexa Fluor 565-ILB4 at 10 μg/ml in PBS with 1 mmol/L $CaCl_2$ (PBS + Ca) overnight at 4°C, rinsed with PBS + Ca, incubated in PBS + Ca with 1% Triton X-100 for 20 minutes, and washed three times for 5 minutes in PBS + Ca. Images were collected on an Olympus (Center Valley, PA) FV500 laser-scanning confocal microscope using a ×4 objective.

For immunostaining of flat mounts, unfixed eyes were dissected, flat mounts prepared and fixed on the slide by immersion in 100% methanol at −20°C for 5 minutes. Blocking and incubations were as described[18] using AP255 or rat anti-CD31 (Pharmingen, La Jolla, CA) as primary antibodies and 1:200 dilutions of Alexa Fluor 488 anti-rat (Invitrogen) and Cy3 anti-rabbit (Jackson ImmunoResearch, West Grove, PA) as secondary antibodies. Images were collected on a Zeiss (Thornwood, NY) laser-scanning confocal microscope under ×40 objective using sequential mode to eliminate potential bleed through.

For immunostaining of retinal cross sections, freshly dissected whole eyes were embedded in Tissue Tek and quick-frozen. Frozen sections were prepared and fixed on the slide with methanol at −20°C for 5 minutes. Slides were blocked by incubation in Superblock (Pierce Biochemicals) for 1 hour. All subsequent incubations including primary and secondary antibody incubations (diluted as in previous paragraph) and washes were done in TNT (200 mmol/L NaCl, 50 mmol/L Tris, pH 7.5, 0.1% Tween 20).

Endothelial Cell Culture

Endothelial cells were prepared from mouse heart as reported.[15] Growth medium consisted of Dulbecco's modified Eagle's medium (high glucose, with glutamine and pyruvate) with 20% heat inactivated fetal calf serum, 100 μg/ml heparin, 100 μg/ml endothelial cell growth supplement (Biomedical Technologies, Stoughton MA), 1× nonessential amino acids, 25 mmol/L HEPES, pH 7.4, 15 μg/ml ascorbic acid, 5 μmol/L β-mecaptoethanol, 100 U/ml penicillin, and 0.1 mg/ml streptomycin. Tubulation medium consisted of Dulbecco's modified Eagle's medium (high glucose, with glutamine and pyruvate), 20% heat inactivated fetal calf serum, 50 μmol/L ascorbic acid, 40 ng/ml vascular endothelial growth factor, 40 ng/ml basic fibroblast growth factor (both from R&D Systems, Minneapolis, MN), and 100 nmol/L phorbol 12-myristate 13-acetate. IAA-94 and Bafilomycin A1 (both from Biomol, Plymouth Meeting, PA) were dissolved in dimethyl sulfoxide at 200 mmol/L and 100 μmol/L, respectively, and diluted 1000-fold into medium.

Quantitation of vacuolization was performed with cells grown in 50-μl fibrin gels in 96-well plates. Formalin-fixed, toluidine blue-stained cultures were examined. All cells in all focal planes of randomly selected microscope fields were scored for vacuolization. To be counted as vacuolated, at least one-third of the area of the cell had to be occupied by well-defined vacuolar space. To be counted as multivacuolated, the cell had to contain at least three well-defined vacuoles that together occupied at least one-third of the area of the cell. At least 400 cells were scored at each data point. The experiment was performed three times with independent cell preparations and the results averaged. *P* values were determined using analysis of variance.[20]

Immunostaining Cells in Fibrin Gels

Five μl drops of cell/fibrin suspension were allowed to solidify in eight-well Lab-Tek chambered coverglass (Nunc, Rochester, NY) and incubated in tubulation medium. At 18 hours, the fibrin gel was fixed in PLP (75 mmol/L sodium phosphate, pH 7.4, 75 mmol/L lysine, 10 mmol/L sodium periodate, 2% paraformaldehyde) for 1 hour, permeabilized in Superblock (Pierce Biochemicals) with 0.05% saponin for overnight, incubated with AP255 diluted 1:100 in TNT for 6 hours, washed overnight with four changes of TNT, incubated in 1:200 dilution of cy3 goat anti-rabbit secondary antibody in TNT for 6 hours, and then washed overnight with four changes of TNT.

Vacuolar pH Measurement

Cells were plated in 12-μl fibrin gels in glass-bottomed dishes with fluorescein/tetramethylrhodamine dextran (Invitrogen) at 2 μg/ml in the gel mixture and the tubulation medium. After 8 to 12 hours, plates were mounted on the heated stage of an Olympus FV500 inverted laser-scanning microscope under 5% CO_2 atmosphere. Vacuolated cells were identified under differential interference contrast (DIC) optics. Paired 16-bit images were obtained using a 560- to 600-nm band pass emission filter and with excitation at either 488 or 543 nm. Areas of interest were defined over fluorescently-labeled intracellular compartments and ratio of average fluorescence intensity determined. Average ratios from samples obtained at pH 5.5 and 7.0 in highly buffered, high potassium/nigericin solutions were used to obtain a two point standardization curve for each fibrin gel, which was then used to calculate a pH value for each compartment. Statistical significance between average pH values of each group was determined using Student's unpaired *t*-test.[20]

Results

A new antiserum was raised against a CLIC4 N-terminal peptide. Characterization of the affinity-purified antibody, named AP255, is shown in Figure 1. Western blot of crude bacterial lysates of *Escherichia coli* expressing glutathione *S*-transferase fusion proteins of CLIC1, CLIC4, and CLIC5 probed with AP255 is shown in Figure 1A. The antibody only recognizes the CLIC4 fusion protein (and associated degradation products running as smaller bands). Whole mouse kidney homogenate (which contains CLIC1, CLIC4, and CLIC5) was separated by SDS-PAGE and probed with antibody. A single band with the mobility of CLIC4 was detected and this band disap-

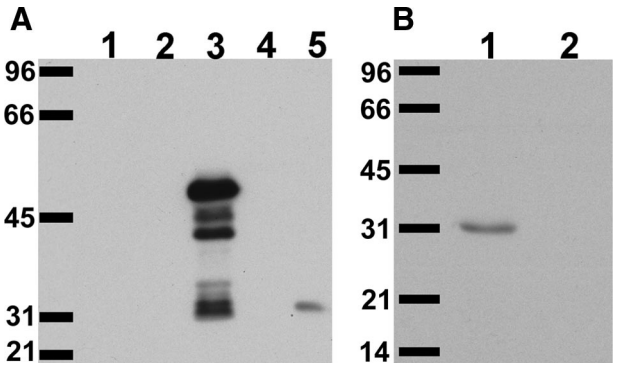

Figure 1. Characterization of AP255 anti-CLIC4 antibody. **A:** Lysates of bacteria expressing glutathione *S*-transferase (GST, **lane 1**) or GST-CLIC1 (**lane 2**), GST-CLIC4 (**lane 3**), or GST-CLIC5 (**lane 4**) fusion protein, or 20 μg of mouse kidney homogenate (**lane 5**) were separated on 10% SDS-PAGE gel, blotted, and probed with a 1:1000 dilution of affinity-purified antibody 255 (AP255). **B:** Twenty μg of mouse kidney homogenate were separated on 12% SDS-PAGE gel, blotted, and probed with a 1:1000 dilution of AP255 either without (**lane 1**) or with (**lane 2**) preabsorption of diluted antibody with the immune peptide at 20 μg/ml for 1 hour prior. Migration positions of molecular weight standards are labeled in kDa. The GST-CLIC4 fusion protein runs at ~50 kDa (with degradation products below); native mouse CLIC4 runs at 31 kDa.

peared with preabsorption of the diluted antibody with antigenic peptide for 1 hour at 20 μg/ml (Figure 1B). Thus, this antibody is specific for CLIC4.

Disruption of Clic4 Gene

A map of the *Clic4* gene, targeting vector, and structure of the recombined chromosomal DNA are shown in Figure 2A. This construct eliminates exon 2 in the recombined product. Splicing from exon 1 to exon 3 would put exon 3 out of frame and introduce a stop codon 84 bases downstream. If the resulting message is stable, the disrupted *Clic4* gene would encode a 5854 MW protein that consists of the N-terminal 24 amino acids of CLIC4 encoded by exon 1, followed by 28 amino acids encoded by the second reading of exon 3 that have no similarity to CLIC4 protein sequence itself.

The targeting vector was used to generate stably-transfected mouse embryonic stem cells. Homologous recombination was confirmed by Southern blotting of *Nhe*I-digested genomic DNA as shown in Figure 2B. Recombinant stem cells were used to generate chimeric mice that were bred with outbred CD-1 mice to generate true heterozygotes. These mice were interbred to generate *Clic4*$^{-/-}$ and wild-type litter mates, which were subsequently bred to each other to generate the lines of *Clic4*$^{-/-}$ and wild-type mice that were used in all experiments. pNT-Cass-loxA vector is designed so that the cassette containing the neomycin gene is eliminated during the first passage through the male germ line.[19,21] Thus, all mice generated from the initial male chimeras contain a deleted gene with only a residual lox-P motif at the site of the deletion. Animals were genotyped by PCR amplification of tail DNA with primers that would yield an 863-bp product from the wild-type gene and an ~240-bp product from the recombinant. Examples of use of PCR to genotype a litter are shown in Figure 2C.

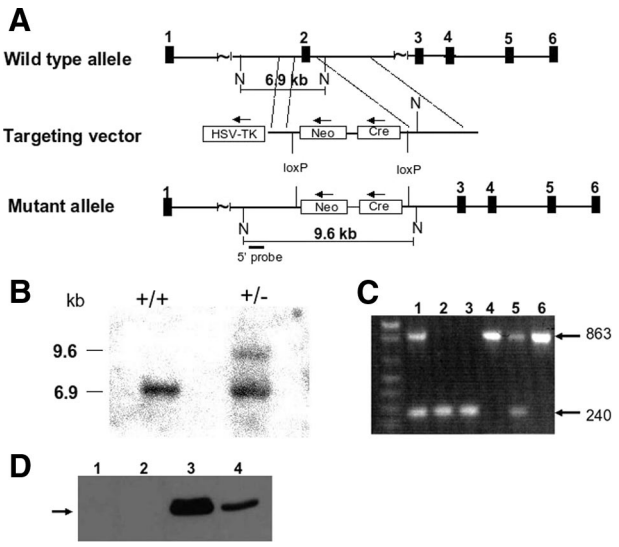

Figure 2. Targeted disruption of the *Clic4* gene. **A:** Structure of the *Clic4* gene (**top**), the targeting construct (**middle**), and the structure of the disrupted *Clic4* gene after homologous recombination (**bottom**). N, *Nhe*I restriction sites; numbered solid boxes, exons; Neo, neomycin resistance cassette; HSV-TK, herpes simplex virus thymidine kinase gene; Cre, cre recombinase gene under control of tACE promoter. The position of the external probe for Southern blotting is indicated. The horizontal lines show the positions of the 6.9- and 9.6-kb restriction fragments diagnostic for wild-type and properly targeted allele, respectively. **B:** Southern blot analysis of *Nhe*I-digested genomic DNA from wild-type ES cells and a recombinant ES line. The blot was hybridized with 5′ external probe. The wild-type and mutant alleles are indicated by 6.9- and 9.6-kb *Nhe*I fragments, respectively. **C:** Tail clip DNA was prepared from members of a litter and used to direct PCR using the genotyping primers. Sizes of the two major amplification products are indicated in bp. The upper band is the product from the wild-type gene, the lower band is the product from the recombinant gene. Resulting CLIC4 genotypes are **lane 1**, +/−; **lane 2**, −/−; **lane 3**, −/−; **lane 4**, +/+; **lane 5**, +/−; **lane 6**, +/+. **D:** Fifty μg of total protein from liver or kidney of CLIC4$^{-/-}$ and wild-type mice was separated by SDS-PAGE and probed with antibody AP1058, specific for CLIC4.[42] **Lane 1:** CLIC4$^{-/-}$ kidney; **lane 2:** CLIC4$^{-/-}$ liver; **lane 3:** wild-type kidney; **lane 4:** wild-type liver. Migration position of the 31-kDa molecular weight standard is indicated by the **arrow**.

Characterization of CLIC4$^{-/-}$ Mice

Total protein and RNA was prepared from wild-type and *Clic4*$^{-/-}$ kidney and liver. Quantitative RT-PCR using a TaqMan 7700 QPCR assay and GAPDH message as the internal standard detected no intact *Clic4* mRNA from the tissues of the *Clic4*$^{-/-}$ mice whereas *Clic4* transcript in the wild-type mice was readily detected. On Western blots of total protein, CLIC4 was undetectable in tissues from the *Clic4*$^{-/-}$ mice (Figure 2D).

Clic4$^{+/-}$ mice were mated and genotypes of 198 consecutive offspring determined, yielding 60 wild type, 110 heterozygotes, and 28 *Clic4*$^{-/-}$. The knockout mice are significantly underrepresented (28 observed, 49.5 predicted; $P < 0.02$). Because the observed number of heterozygotes ($n = 110$) is almost double the observed number of wild-types ($n = 60$) the most direct explanation for the discrepancy is that the *Clic4*$^{-/-}$ embryos have a tendency to prenatal mortality.

Cohorts of littermates from heterozygote crosses were observed for abnormalities in growth and development. *Clic4*$^{-/-}$ mice tend to weigh less than wild-type or heterozygous littermates, but among this cohort, the difference only reached statistical significance among males

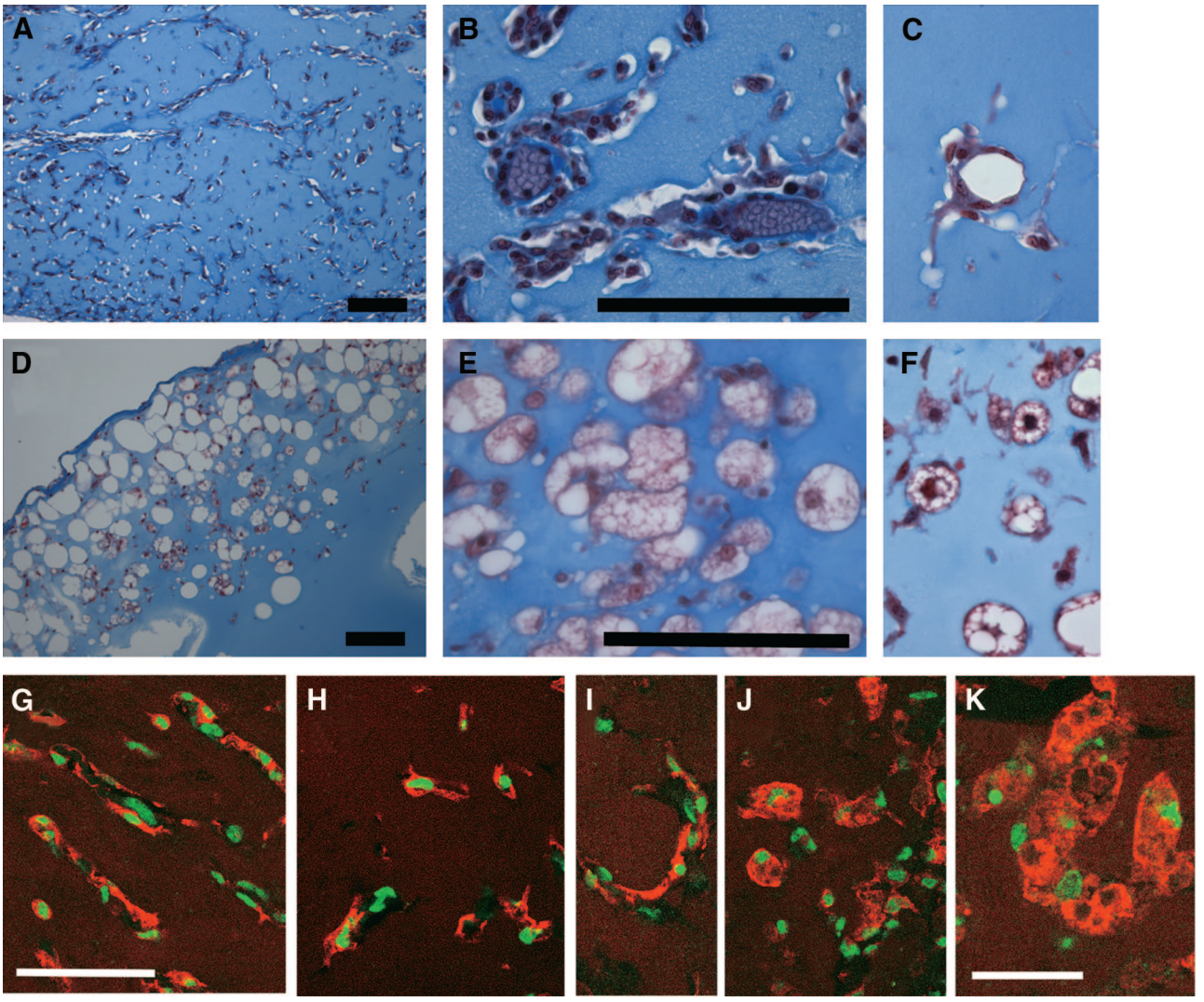

Figure 3. Aberrant Matrigel plug angiogenesis in *Clic4*$^{-/-}$ mice. **A–F:** Trichrome-stained sections of Matrigel plugs imaged with ×10 (**left**) or ×40 (**center** and **right**) objective. **A–C:** Plugs from wild type. **D–F:** Plugs from *Clic4*$^{-/-}$. Note RBC-filled capillaries in **B**, well-formed capillary lumen in **C**, and dilated, vesicle-filled cells in **E** and **F**. **G–K:** Sections of Matrigel plugs stained with the endothelial marker ILB4 (red) and the nuclear marker Sytox Green (green). **G–H:** Plugs from wild-type mice. **I–K:** Plugs from *Clic4*$^{-/-}$ mice. Note the lectin-stained highly vacuolated cells in **J** and **K**. Scale bars: 100 μm (**A**, **B**, **D**, **E**); 50 μm (**G**); 20 μm (**K**).

(at 12 weeks: +/+ males, 39.4 ± 0.9 g, $n = 8$; +/− males, 39.4 ± 1.1, $n = 12$; −/− males, 34.9 ± 1.6 g, $n = 6$; $P < 0.05$ between −/− and either +/− or +/+).

Standard blood and urine chemistries were performed on cohorts of young adults 6 to 12 weeks of age. No systematic differences in serum electrolytes, acid-base status, hemoglobin, urine chemistries, urine volume, or total urine protein were found among the groups of mice. Standard screening histology of a wide range of organs did not identify any structural abnormality. No differences in behavior, spontaneous activity, or gait were noted. The mice appear to have a normal lifespan and do not appear to accumulate any unusual tumors or growths.

Both male and female homozygous knockouts are fertile. However, *Clic4*$^{-/-}$ females have an increased rate of stillbirth among their offspring, independent of the genotype of the father or the offspring. In 15 consecutive litters from 9 different *Clic4*$^{-/-}$ females yielding 111 pups, there were 25 (22.5%) nonviable pups. In contrast, in 12 consecutive litters from wild-type or heterozygous females yielding 146 pups, there was 1 still birth (0.68%). In summary, *Clic4*$^{-/-}$ mice have a modest overt phenotype: they are viable but small, are under-represented among offspring, and females show a high stillbirth rate among their pups.

Matrigel Angiogenesis Assay

We investigated whether *Clic4*$^{-/-}$ mice have a defect in angiogenesis using the Matrigel plug assay.[10,11,22] Four hundred μl of Matrigel supplemented with 200 ng/ml basic fibroblast growth factor were injected subcutaneously. Sections of plugs recovered after 2 weeks from wild-type mice (Figure 3, A–C) show typical features of induced angiogenesis reported by others[12–14]: invading cells form linear structures, some with well-formed lumens that occasionally are filled with red blood cells, demonstrating

that these are vascular structures in continuity with the host's own blood stream. Matrigel plugs from *Clic4*$^{-/-}$ mice show a dramatically different pattern (Figure 3, D–F) with extensive areas filled with large cystic structures that appear to be hugely dilated cells. There are also abundant large multivesicular cells that are very rarely seen in wild type. Almost the entire cytoplasm of these cells appears to be replaced with large dilated vesicles. In addition, some structures similar to those seen in wild-type mice were also found in the plugs from *Clic4*$^{-/-}$ mice. Parallel experiments using vascular endothelial growth factor instead of basic fibroblast growth factor as the inducing agent gave essentially identical results.

To characterize the cells invading the Matrigel further, sections were stained with fluorescently-labeled endothelial-specific marker, isolectin B4 from *G. simplicifolia* (ILB4) and counterstained with the nuclear marker Sytox Green. As expected in plugs from wild-type mice, most of the cells are in linear or tubular structures that stain with the lectin and thus represent developing endothelial cells along the pathway of angiogenesis (Figure 3, G and H). In plugs from *Clic4*$^{-/-}$ mice, some structures similar to those in the wild-type plugs are seen (Figure 3I). In addition, the numerous multivacuolated structures also stain with the lectin, indicating these also represent endothelial structures (Figure 3, J and K).

Hemoglobin content of the Matrigel plugs was used as a measure of angiogenesis.[10,11] As determined by densitometry of Western blots, plugs from wild-type mice contained 431 ± 61 (mean ± SE) arbitrary units of hemoglobin/mg protein ($n = 6$) whereas plugs from *Clic4*$^{-/-}$ animals contained 172 ± 56 ($n = 7$). Overall development of blood-filled vessels was decreased by 60% ($P < 0.01$).

Retinal Vasculature in Clic4$^{-/-}$ *Mice*

To determine whether the absence of CLIC4 affected a naturally occurring vascular bed, we examined the eye.[23] We first determined whether CLIC4 is expressed in the retinal vasculature. Whole mounts of wild-type adult mouse retina were stained with antibodies to both CLIC4 and the endothelial marker, CD31 (Figure 4A), revealing CLIC4 is present in retinal blood vessels. In addition, frozen sections of adult eyes from wild-type and *Clic4*$^{-/-}$ mice were stained for CLIC4 and CD31. The vascular pattern in these cross sections is similar between wild-type and *Clic4*$^{-/-}$ mice with both superficial and deeper capillaries present in both retinas (Figure 4, B and C). CLIC4 clearly co-localizes with CD31 in vessels in the wild-type eye and is absent from the *Clic4*$^{-/-}$ eye.

The superficial vasculature of the mouse retina develops postnatally, expanding from the central retinal vessels to cover the entire retina by approximately postnatal day 7. This primary plexus undergoes further maturation to yield a fully mature retinal vasculature by approximately day 21. Retinal whole mounts were prepared from mice at age 4, 7, and 21 days. The retinal vascular tree was visualized by staining with the endothelial-specific marker, ILB4. Fluorescence images were collected and composites covering the entire retina were generated.

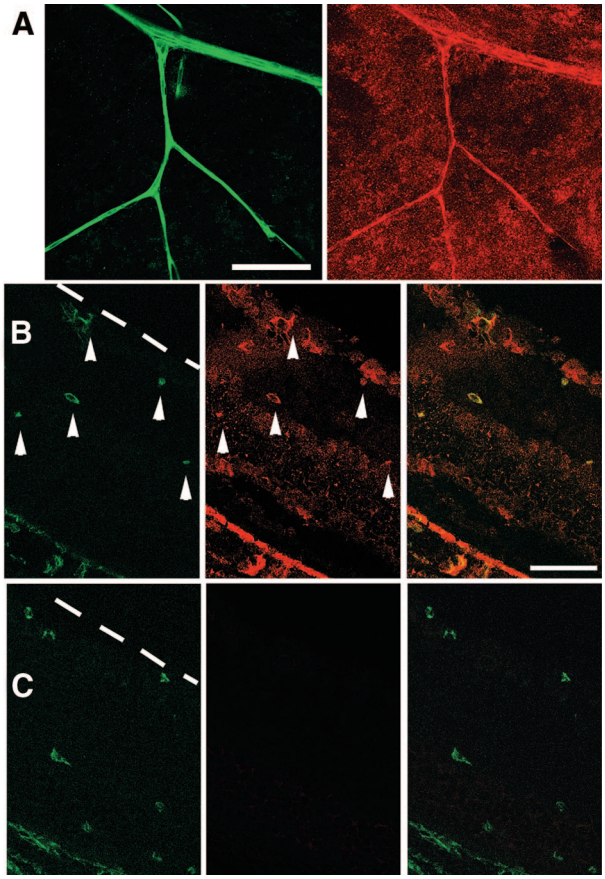

Figure 4. CLIC4 is expressed in retinal blood vessels. Mouse retinas were double stained with AP255, specific for CLIC4 (red) and with antibody to the endothelial marker CD31 (green), and images were collected with confocal fluorescence microscopy. **A:** Whole mount of wild-type retina. There is clear co-localization to retinal surface vessels. **B** and **C:** Frozen sections were prepared from whole eyes and stained as above. The **dotted line** in the green channel image denotes the inner surface of the retina. The rich vascular plexus immediately below the pigmented epithelium is visible in the **bottom left** corner of each image. **B:** Wild-type retina. Cross sections of vessels are marked with **arrowheads**. **C:** *Clic4*$^{-/-}$ retina. Scale bars: 75 μm (**A**); 50 μm (**B**).

Images from day 4 retinas are shown in Figure 5. The amount of retina covered by the advancing vascular tree is approximately comparable between wild-type and *Clic4*$^{-/-}$ mice (Figure 5, A and B). Higher-power images from the advancing edge of the vascular plexus are shown in Figure 5, C–H. Tip cells are seen extending into the peripheral retina in both wild-type and *Clic4*$^{-/-}$ eyes (Figure 5, C and D). Occasional tip cells are seen that appear to contain large intracellular vacuoles. These structures are more easily found in *Clic4*$^{-/-}$ retinas (Figure 5D). Multivacuolated structures very reminiscent of the structures observed in the Matrigel plugs can be found immediately behind the front of the expanding vascular tree (Figure 5, E–H). Although such structures are found in wild-type retinas (Figure 5, E and G), they appear much more abundantly and profusely hypervacuolated in *Clic4*$^{-/-}$ eyes (Figure 5, F and H). These structures are most prominent in a focal plane slightly above that of the vascular tree itself. Figure 5, G and H, shows two images of the identical field taken at two different focal planes. The left image of each pair is in the

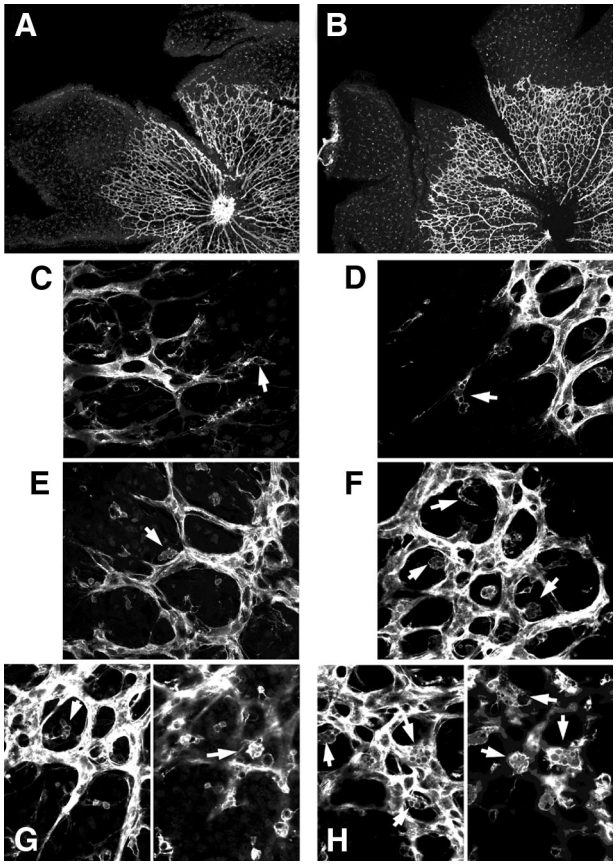

Figure 5. Retinal vasculature of 4-day-old mice. Representative images of retinas from 4-day-old wild-type (**left**) and *Clic4*$^{-/-}$ (**right**) mice stained with ILB4. **A** and **B:** Composite low-power images of wild-type (**A**) and *Clic4*$^{-/-}$ (**B**) retinas. **C** and **D:** High-power images from the leading edge of the vascular plexus from wild-type (**C**) and *Clic4*$^{-/-}$ (**D**) mice. Tip cells (**arrows**) tend to show more prominent vacuolization in *Clic4*$^{-/-}$. **E–H:** Large multivacuolated lectin-stained cells (**arrows**) are visible immediately behind the leading edge of the growing vascular tree, more prominent in the *Clic4*$^{-/-}$ (**F**, **H**) than wild-type (**E**, **G**) eyes. **G** and **H:** Images of a single microscope field from wild-type (**G**) or *Clic4*$^{-/-}$ (**H**) mice are shown at two different focal planes, one focused on the vascular plexus (**left** image of each pair) and one focused ~10 μm higher (**right** image of each pair).

optimal focal plane of the major vascular network. The image to the right of each pair shows the same focal plane focused ~20 μm higher. Although some multivacuolated structures are visible in the focal plane of the vascular network, more abundant, profusely hypervacuolated structures are prominent in the higher plane. These structures are dramatically more prominent in the *Clic4*$^{-/-}$ retinas (Figure 5H) than in the wild type (Figure 5G).

Images of retinas from 7-day-old mice are shown in Figure 6, A and B. At day 7, the primary vascular plexus has spread to cover almost the entire surface of the retina and has begun to mature. Both wild-type and *Clic4*$^{-/-}$ retinas appear approximately comparable, although, the leading edge of the vascular network has reached the end of the retina in the wild-type mice, whereas the vascular network of the *Clic4*$^{-/-}$ mice tend to be a little delayed and have not quite reached the periphery of the retina. As a measure of the extent of vascular development, the radius of the developing vascular network as a fraction of the radius of the entire retina was determined. Among wild-type retinas, the radial fraction

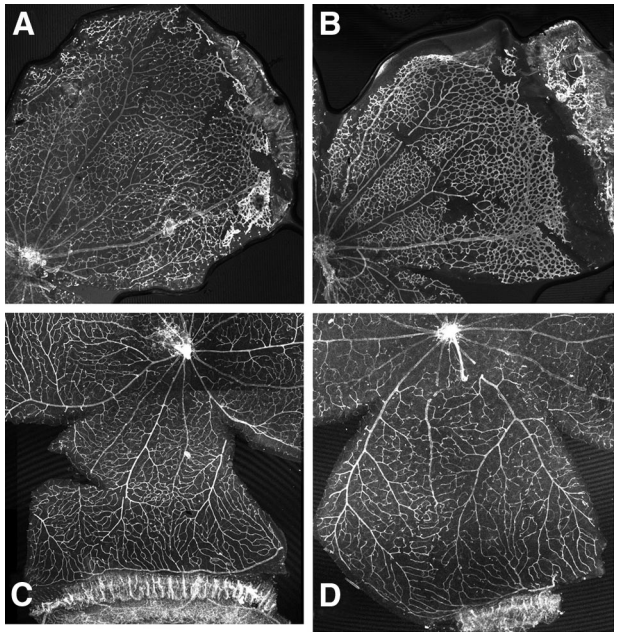

Figure 6. Retinal vasculature at 7 and 21 days. Representative composite low-power images of lectin-stained retinal whole mounts. **A:** Seven-day-old wild type. **B:** Seven-day-old *Clic4*$^{-/-}$. **C:** Twenty-one-day-old wild type. **D:** Twenty-one-day-old *Clic4*$^{-/-}$.

was 0.962 ± 0.008 (n = 7). Among *Clic4*$^{-/-}$ retinas, the radial fraction was 0.857 ± 0.013 (n = 7), the difference being highly significant ($P < 0.00005$).

Images of fully mature retinas from 21-day mice are shown in Figure 6, C and D. The overall patterns appear quite similar between wild-type (Figure 6C) and *Clic4*$^{-/-}$ mice (Figure 6D). Density of the vascular tree was quantified using the angiogenesis module of Metamorph software (Molecular Devices, Sunnyvale, CA). Fraction of the entire area that was comprised of vessels, length of vessels per area, and number of branches per area were determined and averaged among the retinas from each group (Table 1), revealing that the retinal vascular tree in fully developed *Clic4*$^{-/-}$ mice is significantly less dense and complex than that of wild type.

Oxygen toxicity is a stimulus of neoangiogenesis in retinas and is thought to be one cause of the human disease, retinopathy of prematurity.[24] We subjected *Clic4*$^{-/-}$ and wild-type mice to an oxygen-induced retinopathy model in which 7-day-old mice are exposed to 75% oxygen for 5 days followed by recovery for 5 days in normal atmosphere.[13,14] Central retinal capillaries are obliterated during the high constant oxygen exposure followed by intense angiogenesis induced by the relative hypoxia after return to room air. The images in Figure 6, A and B, demonstrate that the retinal vasculature is not dramatically different between wild-type and *Clic4*$^{-/-}$ mice on day 7 at the onset of the hyperoxygen exposure period. Images of retinas from wild-type and *Clic4*$^{-/-}$ mice on day 12 immediately after oxygen exposure are shown in Figure 7, A and B. As is typical for this model of vascular injury, there has been obliteration of the central capillaries with preservation of peripheral vessels. The extent of vascular obliteration is approximately comparable be-

Table 1. Retinal Vascular Density

	Percent area covered	Vessel length (nm/μm^2)	Branch points per 1000 μm^2
Native vessels			
Wild-type, $n = 9$	32.5 ± 1.26	43.6 ± 2.1	1.8 ± 0.12
CLIC4$^{-/-}$, $n = 8$	21.2 ± 0.63	31.5 ± 0.83	1.3 ± 0.05
P value	3×10^{-6}	0.00014	0.00079
After oxygen stress			
Wild-type, $n = 7$	58.8 ± 0.79	56.9 ± 0.73	1.97 ± 0.06
CLIC4$^{-/-}$, $n = 8$	32.4 ± 1.01	38.4 ± 0.94	1.41 ± 0.04
P value	3.7×10^{-11}	2.2×10^{-9}	1.9×10^{-6}

Values were determined for each retina, then averaged to yield the means. Values reported are means ± standard error of mean. *P* values determined with Student's *t*-test.

tween wild-type and *Clic4*$^{-/-}$ retinas. Representative images of retinas on day 17 after recovery from oxygen exposure are shown in Figure 7, C and D. The wild-type mice show a profuse hypervascularity including the typical tufts of preretinal vascular growth into the overlying vitreous humor (prominent in Figure 6C, lower panel). This vascular proliferation is dramatically attenuated in the *Clic4*$^{-/-}$ retinas. The obvious difference in vascular density is born out by the quantitative analysis shown in Table 1, revealing marked attenuation of vascular proliferation in the *Clic4*$^{-/-}$ background.

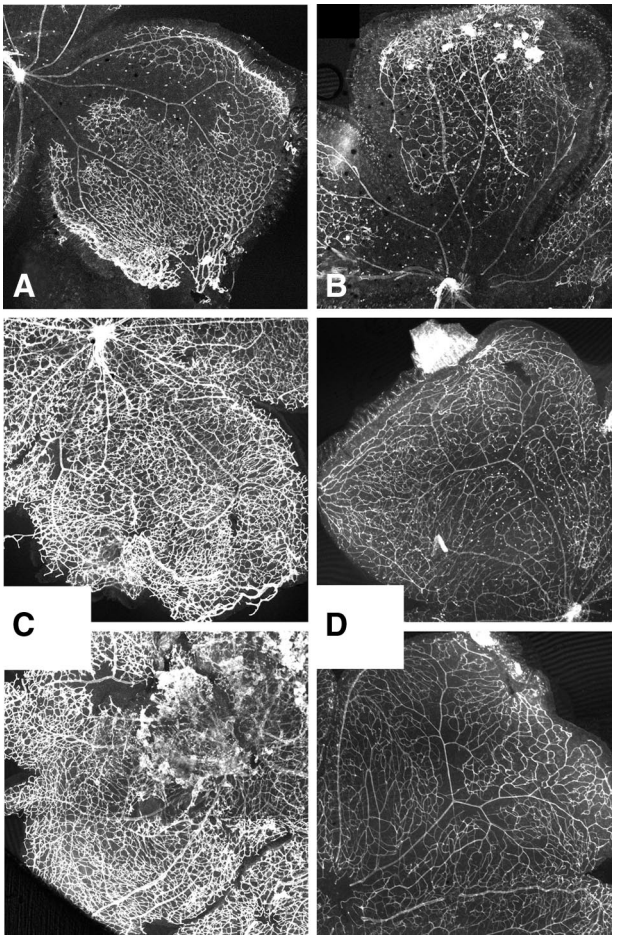

Figure 7. Retinal vascular response to oxygen toxicity. Representative composite low-power images of lectin-stained retinal whole mounts. **A** and **B:** Twelve-day-old wild-type (**A**) and *Clic4*$^{-/-}$ (**B**) after 5 days of high (75%) oxygen exposure. **C** and **D:** Seventeen-day-old wild-type (**C**) and *Clic4*$^{-/-}$ (**D**) after 5 days of 75% oxygen exposure (**upper**) and subsequent 5 days of recovery in room air (**lower**).

Endothelial Tubulogenesis in Culture

Endothelial cells cultured in a three-dimensional matrix can proceed through tubulogenesis with formation and fusion of intracellular vacuoles culminating in multicellular tubes.[16,17,25–28] To determine whether the angiogenesis defect associated with absence of CLIC4 could be detected in cultured cells, primary cultures of mouse heart endothelial cells were prepared[15] and cellular vacuolization/tubulogenesis in fibrin gels was studied as described.[16,17] Typical appearance of toluidine blue-stained cells in fibrin gels are shown in Figure 8. Immediately after plating, both the wild-type (Figure 8A) and *Clic4*$^{-/-}$ (Figure 8B) cells have a simple round ap-

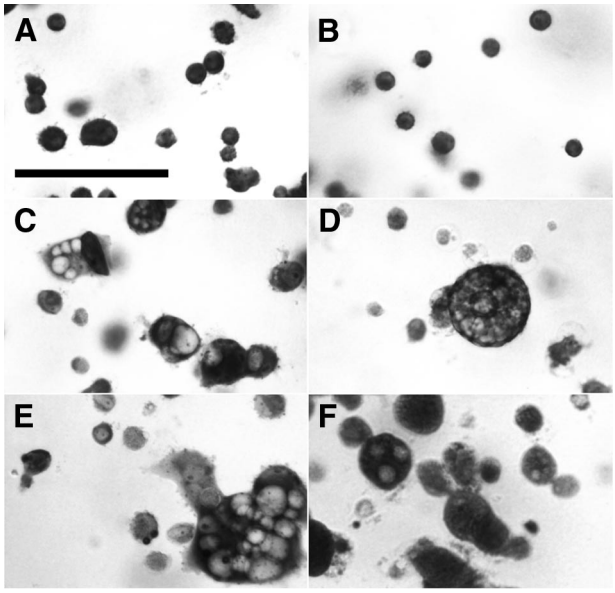

Figure 8. Vacuolization of endothelial cells in fibrin gels. Primary cultures of mouse heart endothelial cells were induced to undergo tubulogenesis in fibrin gels and stained with toluidine blue. **A** and **B:** Wild-type (**A**) and *Clic4*$^{-/-}$ (**B**) cells immediately after plating. Note homogenous populations of small round nonvacuolated cells in both. **C:** Wild-type cells after 16 hours of culture. Small nonvacuolated cells and cells with a single large vacuole or multiple vacuoles are all present. **D:** *Clic4*$^{-/-}$ cells after 16 hours of culture. Fewer cells are vacuolated and multivacuolated cells are more prominent. **E:** Wild-type cells after 16 hours in the presence of 200 μmol/L IAA-94. **F:** Wild-type cells after 16 hours in the presence of 100 μmol/L bafilomycin. Scale bar = 50 μm.

pearance with no obvious intracellular compartment. Throughout several hours, cells acquire large intracellular vacuoles. Most vacuolated cells have one large vacuole occupying almost the entire intracellular space. Other cells accumulate numerous large vacuoles. Typical images of cells after 16 hours of culture are shown for wild-type (Figure 8C) and *Clic4*$^{-/-}$ (Figure 8D) cells. Because the appearance of the wild-type cells becomes extremely heterogeneous as vacuolization progresses, it is difficult to make generalizations about differences in the appearance based on the few cells seen in a single microscopic field. Some cultures were also grown in the presence of the CLIC inhibitor, IAA-94, at 200 μmol/L, or in the presence of the proton ATPase inhibitor, bafilomcyin A1 at 100 μmol/L. Images of toluidine blue-stained cultures at 16 hours in the presence of these inhibitors are shown in Figure 8, E and F, respectively.

Fibrin gel cultures were fixed and stained with toluidine blue at various times and scored for vacuolization,[16,17] plotted in Figure 9A. All cells in all focal planes in randomly selected microscope fields were scored; at least 400 cells were scored for each data point. The data shown are the average of three experiments using independent primary cell cultures. Clearly wild-type cells vacuolated more rapidly and completely than CLIC4$^{-/-}$ cells. Vacuolization was inhibited by either IAA-94 or, most dramatically, by bafilomycin.

In addition to overall vacuolization, toluidine blue-stained cultures cells were also scored for presence of multivacuolization, defined as three or more vacuoles per cell. The fraction of vacuolated cells that were multivacuolated by this definition is shown in Figure 9B. At all time points, the *Clic4*$^{-/-}$ cultures had a greater degree of multivacuolation than did the wild-type cultures. The cells grown in the presence of the either inhibitor also had a tendency toward multivacuolization, although the differences did not reach statistical significance at all time points.

Cultures were immunostained for CLIC4 and images collected by confocal microscopy as shown in Figure 10. Paired DIC and immunofluorescence images are shown. CLIC4 co-localizes with the membranes surrounding the large vacuoles in wild-type cells (Figure 10A). Similar vacuolar structures are found in *Clic4*$^{-/-}$ cells, but as expected these are less common and there is no staining for CLIC4 (Figure 10B). The appearance of wild-type cells grown in the presence of IAA-94 (not shown) was indistinguishable from cells without the drug except that vacuolated cells were less common. Typical images of wild-type cells grown in the presence of bafilomycin are shown in Figure 10C. Some vacuolated cells are present that are similar to cells in the absence of bafilomycin (Figure 10C, left panel). In addition, some larger cells accumulate numerous small vacuoles that stain only weakly for CLIC4 (Figure 10C, right panel). Cells of this appearance are not seen in the absence of bafilomycin. Cells like the one in Figure 10C, right panel, would probably not have been perceived as multivacuolated with toluidine blue stain because the vacuoles are so small.

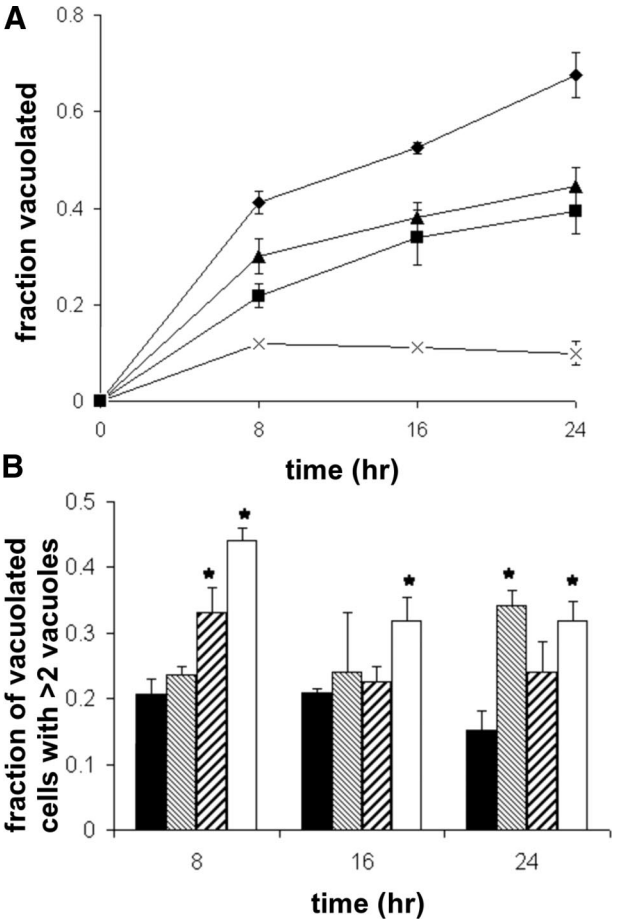

Figure 9. Time course of endothelial cell vacuolization in culture. Endothelial cells were cultured in fibrin gels, fixed at various time points, stained with toluidine blue, and observed under light microscopy. The fraction of total cells vacuolated and fraction of vacuolated cells containing three or more vacuoles were determined. **A:** Plot of fraction of cells vacuolated throughout time. Results shown are averages from three independent experiments performed with different cell preparations. Diamonds, wild-type cells; squares, *Clic4*$^{-/-}$ cells; triangles, wild-type cells grown in the presence of 200 μmol/L IAA-94; crosses, wild-type cells grown in the presence of 100 nmol/L bafilomycin. Error bars represent SE of mean. Error bars smaller than the symbols are not visible. $P < 0.05$ for comparisons between wild-type and all other groups at all points. **B:** Fraction of vacuolated cells that contained three or more clearly distinguishable vacuoles at each time point. Values are averaged from three independent experiments. Solid bars, wild-type cells; fine hatched bars, wild-type with IAA-94; coarse hatched bars, wild-type with bafilomycin; open bars, *Clic4*$^{-/-}$ cells. Error bars represent SEM. *$P < 0.05$ when compared with wild type. Significance was determined using analysis of variance.

Endothelial Vacuolar Acidification

One way chloride channels may function in membrane traffic is by supporting acidification by the electrogenic vH-ATPase, but whether vacuoles along the intracellular tubulogenic pathway acidify has not been reported. We measured pH of endothelial vacuoles directly. Large vacuoles of tubulating endothelial cells have been noted to load with extracellular macromolecules.[2,17,25,27,28] We plated endothelial cells in fibrin gels that had been supplemented with a ratiometric pH indicator, fluorescein-tetramethylrhodamine dextran.[29–31] The fluorescence of fluorescein is strongly pH sensitive, quenching at lower pH within the pH range 7.5 to 5.0. The fluorescence of rhodamine is relatively insensitive to pH in

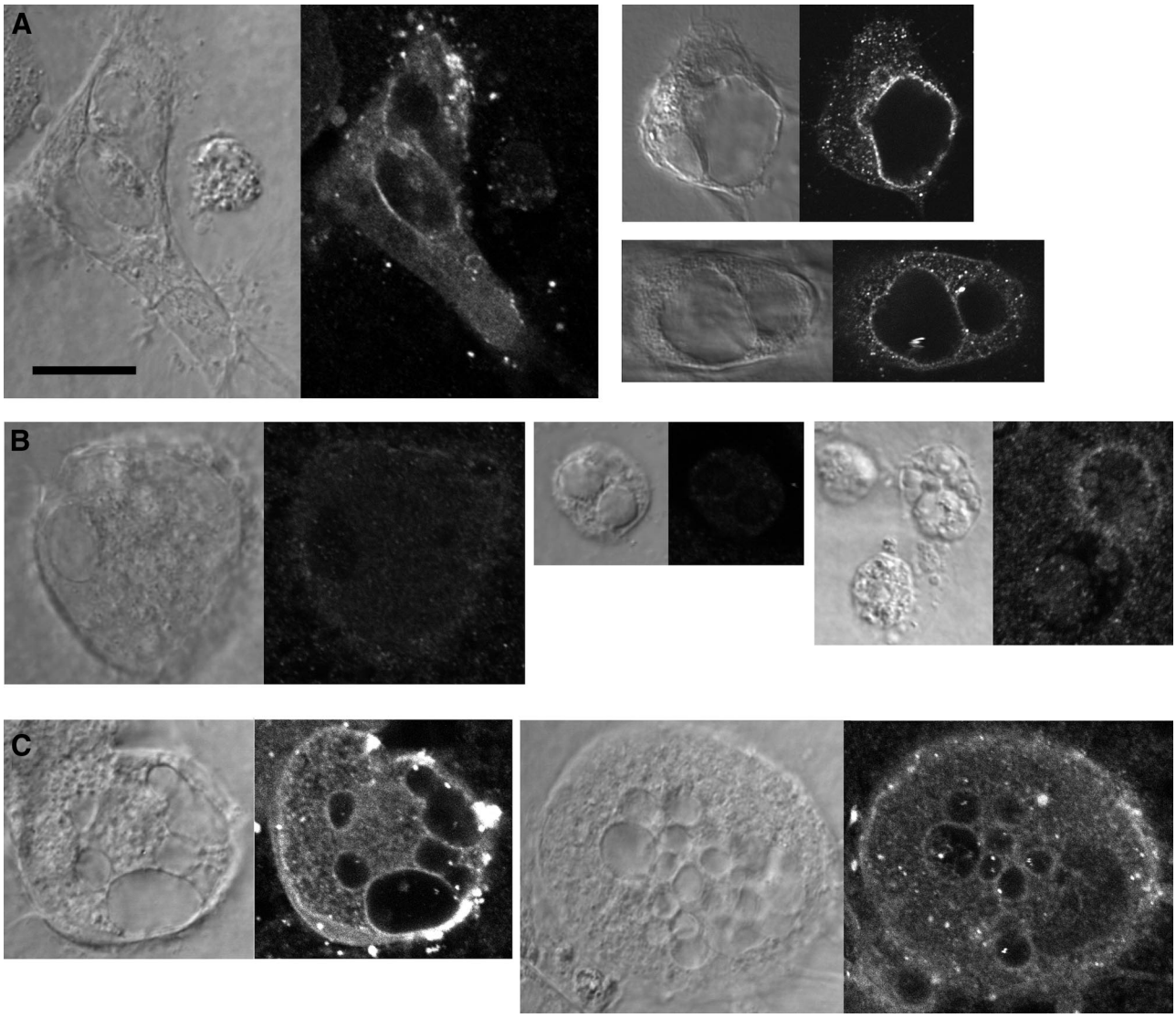

Figure 10. Immunolocalization of CLIC4 in endothelial cells undergoing vacuolization in fibrin gels. Cells were cultured in fibrin gels for 16 hours, fixed, and stained with AP255 antibody to CLIC4. Confocal fluorescent and matching DIC images were obtained. **A:** Wild-type cells. **B:** *Clic4*$^{-/-}$ cells. **C:** Wild-type cells cultured in the presence of 100 nmol/L bafilomycin. Scale bar = 10 μm.

that same range. Therefore, the ratio of fluorescein to rhodamine fluorescence can be used to determine the pH of the environment in which dextran conjugated with both fluorescein and tetramethylrhodamine resides. After 8 to 12 hours of culture, cells were assessed under confocal microscopy. Typical vacuolated wild-type cells loaded with dextran are shown in Figure 11, A–C, and a typical dextran-loaded *Clic4*$^{-/-}$ cell is shown in Figure 11D. The absence of fluorescence in the cytoplasm indicates the dextran has been excluded from the cell as expected. Punctate fluorescent compartments in the cells are consistent with the endosomal/lysosomal pathway, which is expected to load with an extracellular fluid phase marker. The large vacuoles show variable loading with dextran: some vacuoles are efficiently loaded (examples in Figure 11, A–D), some contain dextran at lower concentration than in the extracellular space (see vacuoles to the right in Figure 11B), and some appear not to be loaded with dextran at all (Figure 11C). This variability of loading was observed with both wild-type and *Clic4*$^{-/-}$ cells. Paired fluorescence images were obtained with excitation at 488 or 543 nm and with emission detected using a 560- to 590-nm band pass filter. The fluorescence intensity ratio was determined over labeled intracellular compartments. A standard curve for the relationship between pH and fluorescence intensity ratio in our system is shown in Figure 11E. A two-point standard curve was generated for each fibrin gel and the pH of each intracellular compartment determined. The large vacuoles (minimum greater than 4 μm diameter; most vacuoles analyzed were greater than 10 μm) and the small endosomal/lysosomal compartments (less than 2 μm diameter) were analyzed separately. The experiment was performed three times and results pooled.

In wild-type cells, the average pH of the large vacuoles was 6.75 $\pm$ 0.034 (n = 145) and of the small vesicles was 5.43 $\pm$ 0.033 (n = 146). In *Clic4*$^{-/-}$ cells, the average pH

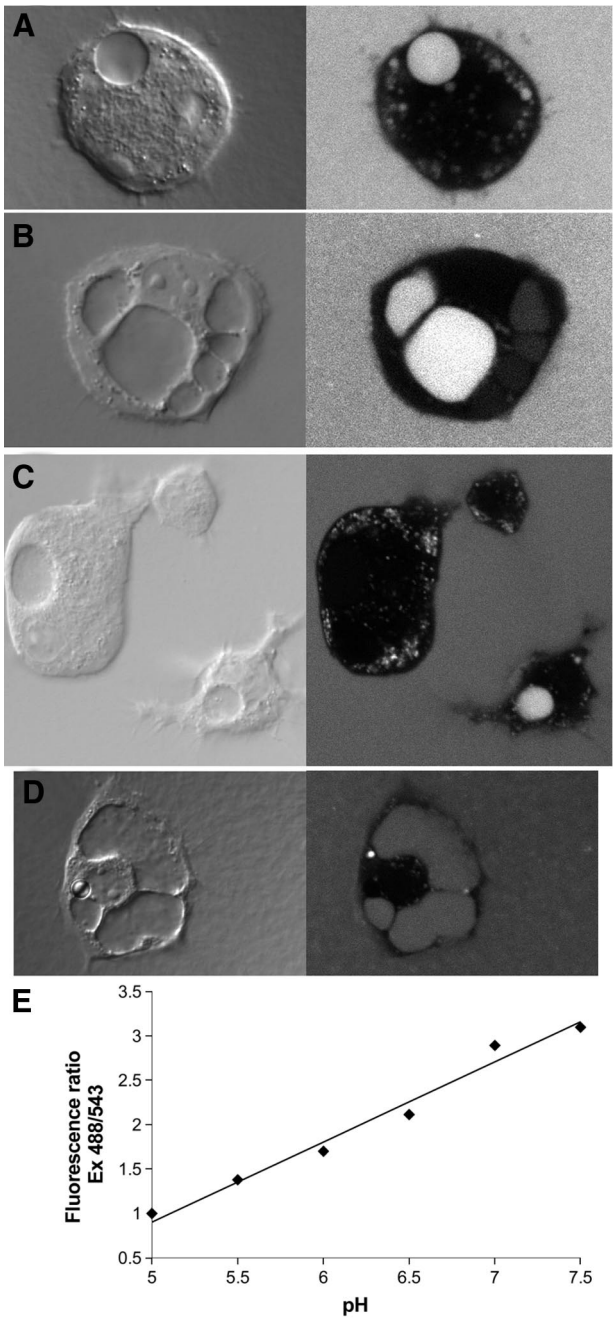

Figure 11. Loading of endothelial vacuoles with pH-sensitive dextran. Cells were grown in fibrin gels supplemented with fluorescent dextran for 8 to 12 hours. **A–C:** Paired DIC (**left**) and confocal fluorescence (**right**) images of wild-type cells are shown. Large vacuoles are obvious in the DIC images and show variable loading with dextran. Abundant, much smaller endosomal/lysosomal structures are also apparent. **D:** *Clic4*$^{-/-}$ cell loaded with dextran and imaged as above. **E:** Relationship between pH and fluorescence ratio from one fibrin gel. All panels are printed at the same magnification. The vertical dimension of panel A is 50 microns.

of large vacuoles was 7.06 ± 0.036 (n = 112) and the pH of the small vesicles was 5.42 ± 0.031 (n = 108). The difference between the pH of the large vacuoles of wild-type and *Clic4*$^{-/-}$ cells is highly significant ($P < 10^{-8}$) whereas the difference between the pH of the small vesicles is not significant (P = 0.75). Thus, large vacuoles along the endothelial tubulogenesis pathway acidify and this acidification is attenuated in *Clic4*$^{-/-}$ cells. In contrast, lysosomal/endosomal acidification is preserved in *Clic4*$^{-/-}$ cells.

Discussion

These experiments lead to several novel conclusions. First, *Clic4*$^{-/-}$ mice are viable and have a minimal phenotype in unstressed conditions, but show increased embryonic lethality (~50%), have defective spontaneous development of blood vessels in the retina with decreased density of retinal vessels in the adult, and show attenuated response to two different models of induced angiogenesis *in vivo*. Second, both the Matrigel and the day 4 retina staining reveal an accumulation of multivacuolated cells in the *Clic4*$^{-/-}$ mice that are reminiscent of the multivacuolated secretory cells of the *C. elegans* CLIC mutant, suggesting they may represent unfused vacuolar precursors of the mature intracellular tube. Third, CLIC4 is present in the membranes of wild-type endothelial vacuoles. Fourth, *Clic4*$^{-/-}$ endothelial cells demonstrate impaired vacuolization that is reproduced in the wild-type cells by a CLIC inhibitor. Fifth, endothelial vacuoles acidify and vacuolization is inhibited by a vH-ATPase inhibitor, indicating that acidification is important for tubulogenesis. Sixth, endothelial cells from *Clic4*$^{-/-}$ mice demonstrate impaired acidification of their large intracellular vacuoles whereas acidification of the small endosomal/lysosomal compartments is intact. Taken together, these data support the hypothesis that the selective failure to acidify the vacuoles along the tubulogenic pathway is the mechanism by which absence of CLIC4 impairs angiogenesis.

We conclude that CLIC4 plays an important role in angiogenesis by supporting intracellular vacuolar fusion and perhaps formation in tubulating endothelial cells at least in part through allowing acidification of the intracellular vacuoles. The absence of CLIC4 impairs ability to proceed with intracellular tubulogenesis and is manifested as an attenuated response to angiogenic challenges accompanied by an accumulation of multivacuolated endothelial intermediates that have been unable to rapidly pass through the tubulogenic program. However, the mildness of the phenotype in mice that survive gestation as well as the fact that any *Clic4*$^{-/-}$ mice are viable, indicates clearly that angiogenesis can occur in the absence of CLIC4.

Functional redundancy among CLIC family members may account for the mildness of the *Clic4*$^{-/-}$ phenotype. Each of the two CLICs encoded by *C. elegans* is able to support tubulogenesis and only cell-specific expression prevents functional complementation *in vivo*.[6,32] In mammals, CLIC1 is widely expressed in virtually all tissues and cell types and is present in primary cultures of mouse endothelial cells (not shown). Our hypothesis is that functional redundancy between CLIC4 and other CLICs is adequate to allow a fraction of *Clic4*$^{-/-}$ mice to survive through embryogenesis to birth and to allow essentially normal postnatal growth and development in the unstressed laboratory environment. However, when angiogenesis is maximally stimulated, as in the Matrigel or the oxygen-stressed retinal

experiments, and perhaps during intrauterine development, a defect in angiogenic capacity is unmasked because of inadequate CLIC activity to support this accelerated pace of angiogenesis. The accumulation of cells filled with unfused vesicles indicates that vesicle fusion may be the rate limiting step of angiogenesis in the *Clic4*$^{-/-}$ milieu. In addition, the decreased overall rate of vacuolization in the cultured cells suggests that CLIC4 might contribute to *de novo* vacuole formation as well as vacuole fusion.

Our data indicate that CLIC4 functions by supporting acidification of vacuoles. However, other possible roles for CLIC4 are not excluded. Chloride channels could also contribute to vesicle trafficking through mass transfer of salt into vesicles driving osmotic vesicle swelling,[33–36] although a necessary role for this process in general intracellular membrane traffic has never been proven. In addition, CLICs have been proposed to be involved in a variety of protein-protein interactions. Identified binding partners for CLICs include a variety of proteins involved in membrane traffic and the cytoskeleton.[37–41] Undoubtedly recruitment of components of the membrane fusion machinery and dynamic regulation of the cytoskeleton must play an important roles in endothelial tubulogenesis. Whether CLIC4 contributes through these mechanism remains to be explored.

Based on the observation that the vacuoles of tubulating endothelial cells can be loaded with extracellular fluid phase markers, it has been suggested that vacuoles along the endothelial tubulogenesis pathway arise from pinocytosis.[25,28] However, simple pinocytosis followed by fusion cannot account for our observation that many vacuoles load poorly or not at all when cells are grown continuously in the presence of fluorescent dextran. Because the dextran is homogeneously present in the extracellular space during the entire time of vacuole formation, these nonloaded vacuoles must either have extruded the dextran after pinocytosis (seemingly unlikely), or else they arose from intracellular vesicles that were not the products of endocytosis/pinocytosis and thus did not contain the extracellular fluid phase marker. However, if the vacuoles do not arise from primary pinocytosis, how does that fraction of vacuoles that do load acquire the dextran? Of course, one possibility is that the origin of the vacuoles is heterogeneous, some vacuoles arising from pinocytosis, some from fusion of nonpinocytic vesicles. A second possible mechanism by which extracellular components could get into these vacuoles would be that vacuoles first form from a nonpinocytic mechanism and then transiently fuse with the plasma membrane during their subsequent maturation. This event would be analogous to the final irreversible fusion with the plasma that must occur as the vacuole becomes the extracellular lumen of the new capillary,[28] the primary difference being that it would be transient rather than irreversible. This mechanism would also be consistent with our observation that the fraction of large vacuoles that are not loaded with dextran decreases with time of incubation (not shown). Thus, although our data do not firmly identify an alternative pathway, these experiments are clearly inconsistent with the hypothesis that the vacuoles of tubulating endothelial cells arise exclusively from simple pinocytosis.

In conclusion, we show that CLIC4 plays an important role in angiogenesis by supporting acidification of vacuoles along the cell-hollowing tubulogenic pathway. The identification of a chloride channel as a component of the cellular basis for angiogenesis opens new avenues for identifying potential therapeutic agents for diseases in which angiogenesis plays a critical role.

Acknowledgments

We thank Dr. Robert Bagnell of the Microscopy Services Laboratory, Department of Pathology and Laboratory Medicine, University of North Carolina, for assitance with microscopy; and the Cell Services and Histology Core of the Center for Gastrointestinal Biology and Disease at the University of North Carolina for providing histology preparation services.

References

1. Lubarsky B, Krasnow MA: Tube morphogenesis: making and shaping biological tubes. Cell 2003, 112:19–28
2. Kamei M, Saunders WB, Bayless KJ, Dye L, Davis GE, Weinstein BM: Endothelial tubes assemble from intracellular vacuoles in vivo. Nature 2006, 442:453–456
3. Béraud-Dufour S, Balch W: A journey through the exocytic pathway. J Cell Sci 2002, 115:1779–1780
4. Mellman I: The importance of being acid: the role of acidification in intracellular membrane traffic. J Exp Biol 1992, 172:39–45
5. Ashley RH: Challenging accepted ion channel biology: p64 and the CLIC family of putative intracellular anion channel proteins. Mol Membr Biol 2003, 20:1–11
6. Berry KL, Bulow HE, Hall DH, Hobert O: AC. elegans CLIC-like protein required for intracellular tube formation and maintenance. Science 2003, 302:2134–2137
7. Bohman S, Matsumoto T, Suh K, Dimberg A, Jakobsson L, Yuspa S, Claesson-Welsh L: Proteomic analysis of vascular endothelial growth factor-induced endothelial cell differentiation reveals a role for chloride intracellular channel 4 (CLIC4) in tubular morphogenesis. J Biol Chem 2005, 280:42397–42404
8. Tulk BM, Schlesinger PH, Kapadia SA, Edwards JC: CLIC-1 functions as a chloride channel when expressed and purified from bacteria. J Biol Chem 2000, 275:26986–26993
9. Bowman EJ, Siebers A, Altendorf K: Bafilomycins: a class of inhibitors of membrane ATPases from microorganisms, animal cells, and plant cells. Proc Natl Acad Sci USA 1988, 85:7972–7976
10. Albig AR, Neil JR, Schiemann WP: Fibulins 3 and 5 antagonize tumor angiogenesis in vivo. Cancer Res 2006, 66:2621–2629
11. Yi M, Sakai T, Fassler R, Ruoslahti E: Antiangiogenic proteins require plasma fibronectin or vitronectin for in vivo activity. Proc Natl Acad Sci USA 2003, 100:11435–11438
12. McColm JR, Geisen P, Peterson LJ, Hartnett ME: Exogenous leukemia inhibitory factor (LIF) attenuates retinal vascularization reducing cell proliferation not apoptosis. Exp Eye Res 2006, 83:438–446
13. Smith LE, Wesolowski E, McLellan A, Kostyk SK, D'Amato R, Sullivan R, D'Amore PA: Oxygen-induced retinopathy in the mouse. Invest Ophthalmol Vis Sci 1994, 35:101–111
14. Chikaraishi Y, Shimazawa M, Hara H: New quantitative analysis, using high-resolution images, of oxygen-induced retinal neovascularization in mice. Exp Eye Res 2007, 84:529–536
15. Lim YC, Garcia-Cardena G, Allport JR, Zervoglos M, Connolly AJ, Gimbrone Jr MA, Luscinskas FW: Heterogeneity of endothelial cells from different organ sites in T-cell subset recruitment. Am J Pathol 2003, 162:1591–1601
16. Bayless KJ, Salazar R, Davis GE: RGD-dependent vacuolation and lumen formation observed during endothelial cell morphogenesis in three-dimensional fibrin matrices involves the alpha (v) beta(3) and alpha(5)beta(1) integrins. Am J Pathol 2000, 156:1673–1683
17. Bayless KJ, Davis GE: The Cdc42 and Rac1 GTPases are required

for capillary lumen formation in three-dimensional extracellular matrices. J Cell Sci 2002, 115:1123–1136
18. Ulmasov B, Bruno J, Woost PG, Edwards JC: Tissue and subcellular distribution of CLIC1. BMC Cell Biol 2007, 8:8
19. Shah N, Ulmasov B, Waheed A, Becker T, Makani S, Svichar N, Chesler M, Sly WS: Carbonic anhydrase IV and XIV knockout mice: roles of the respective carbonic anhydrases in buffering the extracellular space in brain. Proc Natl Acad Sci USA 2005, 102:16771–16776
20. Armitage P: Statistical Methods in Medical Research, ed 4. Oxford, Blackwell Scientific Publications, 1971, pp 99–216
21. Bunting M, Bernstein KE, Greer JM, Capecchi MR, Thomas KR: Targeting genes for self-excision in the germ line. Genes Dev 1999, 13:1524–1528
22. Auerbach R, Lewis R, Shinner B, Kubai L, Akhtar N: Angiogenesis assays: a critical overview. Clin Chem 2003, 49:32–40
23. Uemura A, Kusuhara S, Katsuta H, Nishikawa S: Angiogenesis in the mouse retina: a model system for experimental manipulation. Exp Cell Res 2006, 312:676–683
24. Chen J, Smith LE: Retinopathy of prematurity. Angiogenesis 2007, 10:133–140
25. Davis GE, Camarillo CW: An alpha 2 beta 1 integrin-dependent pinocytic mechanism involving intracellular vacuole formation and coalescence regulates capillary lumen and tube formation in three-dimensional collagen matrix. Exp Cell Res 1996, 224:39–51
26. Bach TL, Barsigian C, Chalupowicz DG, Busler D, Yaen CH, Grant DS, Martinez J: VE-cadherin mediates endothelial cell capillary tube formation in fibrin and collagen gels. Exp Cell Res 1998, 238:324–334
27. Yang S, Graham J, Kahn JW, Schwartz EA, Gerritsen ME: Functional roles for PECAM-1 (CD31) and VE-cadherin (CD144) in tube assembly and lumen formation in three-dimensional collagen gels. Am J Pathol 1999, 155:887–895
28. Davis GE, Bayless KJ: An integrin and Rho GTPase-dependent pinocytic vacuole mechanism controls capillary lumen formation in collagen and fibrin matrices. Microcirculation 2003, 10:27–44
29. Zen K, Biwersi J, Perisasamy N, Verkman A: Second messengers regulate endosomal acidification in Swiss 3T3 fibroblasts. J Cell Biol 1992, 119:99–110
30. van Weert AWM, Dunn KW, Gueze HJ, Maxfield FR, Stoorvogel W: Transport from late endosomes to lysosomes, but not sorting of integral membrane proteins in endosomes, depends on the vacuolar proton pump. J Cell Biol 1995, 130:821–834
31. Haughland RP: Handbook of Fluorescent Probes and Research Products, ed 9. Eugene, Molecular Probes, 2002, p 844
32. Berry KL, Hobert O: Mapping functional domains of chloride intracellular channel (CLIC) proteins in vivo. J Mol Biol 2006, 359:1316–1333
33. Gasser KW, DiDomenico J, Hoper U: Secretatgogues activate chloride transport pathways in pancreatic zymogen granules. Am J Physiol 1988, 254:G93–G99
34. Dayanithi G, Nordmann JJ: Chloride and magnesium dependence of vasopressin release from rat permeabilized neurohypophysial nerve endings. Neurosci Lett 1989, 106:305–309
35. Fuller CM, Eckhardt L, Schultz I: Ionic and osmotic dependence of secretion from permeabilized acini of the rat pancreas. Pflugers Arch 1989, 413:385–394
36. Takuma T, Ichida T: Roles of potassium and chloride ions in cAMP-mediated amylase exocytosis from rat parotid acini. Cell Struct Funct 1991, 16:405–409
37. Berryman M, Bretscher A: Identification of a novel member of the chloride intracellular channel gene family (CLIC5) that associates with the actin cytoskeleton of placental microvilli. Mol Biol Cell 2000, 11:1509–1521
38. Edwards JC, Kapadia S: Regulation of the bovine kidney microsomal chloride channel p64 by p59fyn, a src family tyrosine kinase. J Biol Chem 2000, 275:31826–31832
39. Suginta W, Karoulias N, Aitkin A, Ashley RH: Chloride intracellular channel protein CLIC4 (p64H1) binds directly to brain dynamin I in a complex containing actin, tubulin and 14–3–3 isoforms. Biochem J 2001, 359:55–64
40. Shanks RA, Larocca MC, Berryman M, Edwards JC, Urushidani T, Navarre J, Goldenring JR: AKAP350 at the Golgi apparatus. J Biol Chem 2002, 277:40973–40980
41. Park JS, Lee KM, Jeong MS, Jin GE, Jang SB: The binding of human CLIC1 with SEDL and its characterization in vitro. Bull Korean Chem Soc 2007, 28:574–580
42. Edwards JC: A novel member of the p64 Cl channel family: subcellular distribution and nephron segment-specific expression. Am J Physiol 1999, 276:F398–F408